



## Temperature Field Analysis of High-Speed Bearings Considering Frictional Heat and Interactive Effects

Xin Zheng 

School of Intelligent Manufacturing, Zibo Vocational Institute, Zibo 255300, China

Corresponding Author Email: [10672@zbvc.edu.cn](mailto:10672@zbvc.edu.cn)

<https://doi.org/10.18280/ijht.410215>

### ABSTRACT

**Received:** 20 December 2022

**Accepted:** 17 March 2023

#### Keywords:

*frictional heat generation, thermal interaction, high-speed bearings, temperature field analysis*

The temperature of bearings has a significant impact on their service life and flexibility, so it becomes more important to analyze the temperature field of bearings in high-speed electric spindle machining applications. Scholars at home and abroad have completed the thermal characteristics analysis of high-speed bearings from multiple perspectives such as frictional heat generation, heat transfer, and thermal analysis, but there is less consideration of the effects of spin, rotation speed, and external loads on the temperature field, and the complex motion between various components inside the bearing is also ignored. There are even fewer transient thermal analyses of high-speed bearings using the ANSYS finite element analysis method. Therefore, this paper carries out a temperature field analysis of high-speed bearings considering the interactive effects of frictional heat generation. Firstly, the motion laws of bearings and the mechanism of friction generation are analyzed, and a high-speed bearing frictional heat generation calculation analysis model that conforms to actual working conditions is established. Based on the ANSYS finite element analysis software, the temperature field of high-speed bearings is analyzed, and the internal temperature field distribution law is obtained by exploring the effects of spin, rotation speed, and external loads on their temperature field. Finally, the paper presents experimental analysis results, which verify the effectiveness of the proposed calculation method and the established model.

## 1. INTRODUCTION

During the operation of high-speed machine tools, spindle bearings rotate at high speeds with the electric spindle, and various friction factors generate resistance torque, intensifying internal frictional heat generation in the bearings [1-7]. If the bearing friction torque is too large, the temperature of the bearing will increase significantly, the lubrication performance of non-circulating grease will be greatly reduced, relative thermal displacement will occur inside the bearing components, and it is easy to cause surface burns on internal components, leading to bearing failure, damage, or even premature scrapping [8-13]. The temperature of the bearing has a significant impact on its service life and flexibility, and the deformation of components caused by friction factors also seriously affects the accuracy and stability of machined parts [14-20]. Therefore, it is more important to analyze the temperature field of bearings in high-speed electric spindle machining applications.

Regarding the uneven heating problem of ultra-high molecular weight polyethylene (UHMWPE) bearings during the preparation of water-lubricated bearings, Chen et al. [21] used ICEPAK software to study the temperature distribution of UHMWPE bearings during the hot pressing process. The study showed that the non-steady-state heat transfer occurs during the heating and heat preservation processes of hot-pressed UHMWPE. Air convection has almost no effect on the entire process. This research can provide data support for temperature control and process optimization of UHMWPE-

based water-lubricated bearing hot pressing process. The rheological properties of grease have an important impact on bearing heating and heat transfer. However, due to the combined effects of shear rate, temperature, and load, there are few studies on bearing temperature fields considering the rheological properties of grease. Wang et al. [22] used the Bausser four-parameter model to describe the rheological properties of grease, calculated the heat generation of bearings under grease lubrication conditions, and considered the effects of different grease base oil viscosities. Finite element analysis of the bearing temperature field was conducted, and the influence of plastic viscosity and shear rate on heat generation and heat distribution working conditions was studied. The results showed that there is a significant difference in the heat generation of bearings under different grease lubrication conditions when considering the rheological properties of grease. Intelligent bearings are one of the research and development directions of high-end bearings at home and abroad. Chen et al. [23] studied the structural design issues related to the integration of rolling bearings and sensors based on a finite element model. According to the load distribution of the bearing, the optimal groove position of the bearing was determined. Considering the impact of bearing load reduction, the effects of axial and radial grooves on the outer ring on the maximum deformation and stress of the outer ring were studied, and the maximum stress and groove size of the outer ring were determined to provide a basis for the selection and design of sensor modules. Bao et al. [24] established a simplified three-dimensional heat transfer model of lubricated



The calculation formula for  $\gamma$  is as follows:

$$\gamma = \beta \tan \frac{\sin \beta_o}{\alpha' + \cos \beta_o} \quad (5)$$

Since the frictional heat generation of high-speed bearings results from the conversion of the loss power due to the frictional interaction between internal components, this article first calculates the friction torque of the bearing. Assume that the total heat generated by the rolling bearing is represented by  $F$ , the inner ring rotation speed of the bearing is represented by  $m$ , and the friction torque of the bearing is represented by  $N$ . The calculation formula is as follows:

$$F = 1.01 \times 10^{-5} Nm \quad (6)$$

Assuming the friction coefficient of the rolling bearing is represented by  $\lambda$ , the inner diameter of the rolling bearing is represented by  $c$ , the load-bearing capacity of the bearing is represented by  $T$ , and the rated dynamic load of the bearing is represented by  $D$ . When the lubrication performance of the bearing grease is good and the speed and load of the high-speed bearing have not reached their peak, the friction torque can be calculated using the following formula:

$$\begin{aligned} N &= \frac{1}{2} \lambda c T \\ T &\approx 0.1 D \end{aligned} \quad (7)$$

Here, the bearing load  $T$  is the radial load on the centripetal roller bearing or the axial load on the thrust roller bearing. For bearings with both axial and radial loading, if  $G_x/G_s \leq 1.5 \tan \beta$ , then  $T$  is assumed to be the radial load; if  $G_x/G_s > 1.5 \tan \beta$ , then  $T$  is assumed to be the axial load.

As the rotation speed of high-speed bearings increases, the friction torque gradually increases, and the amount of heat generated increases. The following formula gives the calculation formula for bearing friction torque:

$$N = N_0 + N_1 \quad (8)$$

The friction torque of high-speed bearings is greatly affected by the friction torque generated by the spinning and sliding of the rolling elements. Therefore, this paper takes into account the frictional heat generated by the spinning motion of the bearings when performing friction heat generation calculations and analysis for high-speed bearings. In the frictional heat generation analysis of high-speed bearings, we first need to consider the spinning friction torque and the radial load of the bearings. Let the spinning friction torque be represented by  $N_r$ , the radial load between the rolling elements and the raceway be represented by  $W$ , and the long axis width of the contact angle be represented by  $x$ . Based on these parameters, we can calculate the spinning torque:

$$N_r = \frac{3\lambda W x \Sigma}{8} \quad (9)$$

The frictional heat generated between the inner and outer rings and the rolling elements of the bearing is represented by  $F_i$  and  $F_e$ , respectively. The total frictional heat generated in the bearing is represented by  $F$ . The spinning speed of the

rolling elements relative to the inner ring of the bearing is represented by  $\theta_{ri}$ . Based on these parameters, we can calculate the frictional heat generated in the inner and outer rings of the bearing:

$$\begin{aligned} F_i &= \frac{1}{2} \left( \frac{2\pi}{60} m (N_e + N_i) \right) + N_{rp} \theta_{ri} \\ F_o &= \frac{1}{2} \left( \frac{2\pi}{60} m (N_e + N_i) \right) \\ F &= F_i + F_e \end{aligned} \quad (10)$$

When analyzing the temperature field of high-speed bearings, it is necessary to evenly distribute the heat generated by the friction interaction between the rolling elements and the inner and outer rings of the bearing, as well as the heat generated by their spinning friction, in the same proportion to the inner and outer rings and rolling elements. Assume that the heat flux density acting on the outer ring of the high-speed bearing is represented by  $w_e$ , the heat flux density on the inner ring is represented by  $w_i$ , the contact area between the rolling elements and the inner ring is represented by  $X_e$ , and the contact area with the outer ring is represented by  $X_i$ . The formula for calculating the heat source heat flux density on the inner and outer rings of the bearing is as follows:

$$\begin{cases} w_i = \frac{1}{2} \frac{F_i}{X_i} \\ w_e = \frac{1}{2} \frac{F_e}{X_e} \end{cases} \quad (11)$$

In order to accurately calculate the heat generation of high-speed bearings considering the interaction effect of frictional heat, this article constructs a *Palmgren* frictional heat calculation model. Based on the bearing frictional heat analysis results of *ANSYS* finite element analysis software, the total frictional heat generation can be further calculated using *MATLAB* software based on fixed parameter values such as bearing inner diameter, outer diameter, and rotation speed. Figure 2 shows the simulation analysis flowchart of high-speed bearing frictional heat generation.

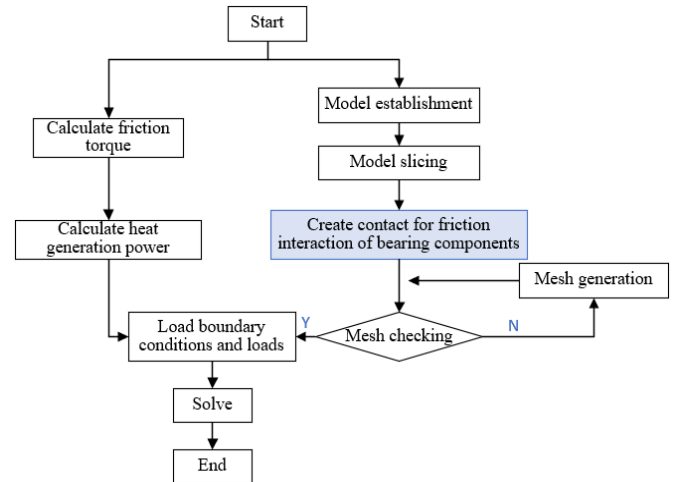


Figure 2. High-speed bearing frictional heat generation simulation analysis flowchart

### 3. TEMPERATURE FIELD ANALYSIS OF HIGH-SPEED BEARINGS

Next, this article will conduct a temperature field analysis of high-speed bearings based on ANSYS finite element analysis software. By exploring the effects of the spin, rotation speed, and external load of high-speed bearings on their temperature field, we can obtain the internal temperature field distribution rules. First, the temperature distribution of high-speed bearings is derived based on the steady-state thermal analysis of ANSYS finite element analysis, and the corresponding finite element control equation is obtained.

Assume that density is represented by  $\sigma$ , specific heat capacity by  $d$ , temperature by  $P$ , time by  $p$ , heat generation rate per unit volume by  $w^*$ , and the thermal conductivity coefficients of unit  $a$ ,  $b$ , and  $c$  directions are represented by  $l_{aa}$ ,  $l_{bb}$ , and  $l_{cc}$ , respectively. The mass heat transfer velocities are represented by  $u_a$ ,  $u_b$ , and  $u_c$ . Based on the first law of thermodynamics and Fourier's law, the following differential control equation for high-speed bearing heat conduction can be constructed:

$$\begin{aligned} \frac{\partial}{\partial a} \left( l_{aa} \frac{\partial P}{\partial a} \right) + \frac{\partial}{\partial b} \left( l_{bb} \frac{\partial P}{\partial b} \right) + \frac{\partial}{\partial c} \left( l_{cc} \frac{\partial P}{\partial c} \right) + w^* \\ = \sigma d \left( \frac{\partial P}{\partial p} + v_a \frac{\partial P}{\partial a} + v_b \frac{\partial P}{\partial b} + u_c \frac{\partial P}{\partial c} \right) \end{aligned} \quad (12)$$

In the actual working conditions of high-speed bearings, it is necessary to fully consider the three boundary conditions of fixed temperature, fixed heat flow, and fixed convection heat transfer. Assume that the overall specific heat capacity matrix is represented by  $[D]$ , the overall thermal conductivity matrix by  $[L_P]$ , and the overall thermal load vector by  $\{W\}$ . Based on the above formula and deriving the boundary conditions, the finite element control equation for high-speed bearing temperature field analysis can be constructed:

$$[D]\{\dot{P}\} + [L_P]\{P\} = \{W\} \quad (13)$$

When the temperature field of high-speed bearings tends to stabilize over time, the above equation can be simplified as follows:

$$[L_P]\{P\} = \{W\} \quad (14)$$

Figure 3 shows the schematic diagram of heat transfer between components inside a high-speed bearing, displaying 9 types of heat transfer modes. Ignoring radiation heat dissipation, it is assumed that high-speed bearings mainly transfer heat through conduction and convection. In order to obtain more accurate bearing temperature field analysis results, it is important to focus on constructing the heat transfer and heat exchange model of high-speed bearings. Since the heat transfer process inside the bearing is relatively simple to calculate, this article focuses on constructing the heat exchange model for high-speed bearings.

For high-speed bearing systems, convective heat transfer can be considered as heat transfer between the thermal fluid and the surfaces of internal components. Assume that the heat exchange amount is represented by  $\Psi$ , the convective heat transfer coefficient by  $f$ , the contact surface area by  $X$ , and the temperature difference between the fluid and solid surface by

$\Delta p$ . The following formula gives the convective heat calculation formula based on Newton's cooling law:

$$\Psi = fX\Delta p \quad (15)$$

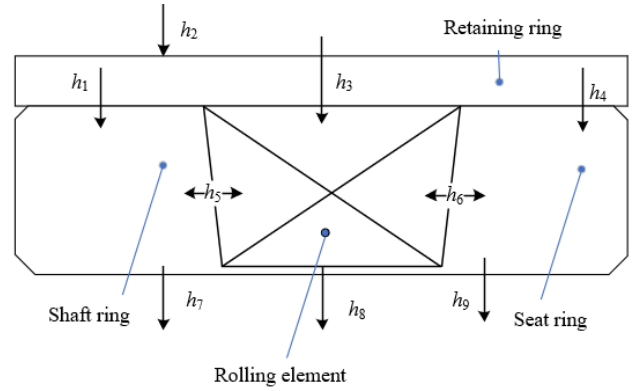


Figure 3. Schematic diagram of heat transfer between components inside a high-speed bearing

In the above formula, the convective heat transfer coefficient  $f$  is difficult to obtain in line with actual values due to the influence of various complex factors, so further discussion on its calculation method is needed.

The calculation of the convective heat transfer coefficient  $f$  needs to be limited by the type of bearing. Assume that the thermal conductivity coefficient and the Prandtl number of the grease are represented by  $l$  and  $P_r$ , respectively, the Reynolds number by  $Re = va/u_0$ , the dynamic viscosity of the grease by  $u_0$ , and when considering the heat transfer between the bearing and the grease, the surface velocity of the bearing cage is represented by  $v$ , the pitch circle diameter by  $a$ . The forced convection heat transfer coefficient for heat transfer from the bearing and the inner wall of the bearing to the grease can be calculated using the following formula:

$$f = 0.315 \frac{l}{a} P_r^{1/3} Re^{1/2}; Re < 5 \times 10^5 \quad (16)$$

Assume that the ambient temperature is represented by  $P_x$ , the outer diameter of the bearing housing by  $C_f$ , the air thermal conductivity coefficient by  $l_x$ ,  $Re = vC_f/u_x$ , the airflow velocity by  $v$ , and the dynamic viscosity of air by  $u_x$ . The following formula provides the convective heat transfer calculation between the bearing housing outer surface and the air:

$$f = \begin{cases} 0.298(P - P_x)^{0.237}, & \text{Natural convection} \\ 0.298 \frac{l_x}{C_f} Re^{0.525}, & \text{Forced convection} \end{cases} \quad (17)$$

Assume that the angular velocity and diameter of the bearing's rotating axis are represented by  $\theta$  and  $c$ , respectively, and the dynamic viscosity of the grease is represented by  $u$ . Simplify the previous two formulas and let  $Re = \pi\theta c^2/u$ . Then, the forced convection heat transfer coefficient calculation formula between the outer surface of the rotating axis and the lubricating oil is as follows:

$$f = 0.11 \frac{l}{c} \left( 0.5NO^2 \cdot GF \right)^{0.35} \quad (18)$$

Assume that the working speed of the rotating ring is represented by  $m$ , and the pitch circle diameter of the bearing is represented by  $c_n$ . Then, the forced convection heat transfer coefficient calculation formula between the lubricating grease and the inner surface of the bearing can be updated as follows:

$$f = 0.0986 \left[ \frac{m}{u} \left( 1 - \frac{C \cos \beta}{c_n} \right) \right]^{1/2} IGF^{1/3} \quad (19)$$

The temperature field of high-speed bearings is influenced by various factors, such as bearing geometry, material properties, working conditions, and lubrication status. The interaction among these factors makes the distribution of the temperature field complex. Using finite element analysis software can better simulate the impact of these complex factors, thus obtaining more accurate results. The method based on ANSYS finite element analysis software can flexibly handle different boundary conditions and material properties, providing effective thermal analysis for different types of high-speed bearings. In addition, this method can conveniently perform parameter sensitivity analysis to identify the key factors affecting the bearing temperature field. The high-speed bearing finite element model constructed in this paper consists of about 15,000 three-dimensional solid elements, 23,000 three-dimensional surface effect elements, and 680,000 nodes.

Two types of loads need to be applied during the bearing temperature field analysis. For the heat flux load, assume that the heat generated by the load on the contact areas of the balls and inner/outer rings is represented by  $F_k$ , the heat generated by the load on the ball surface caused by rolling friction and spin-sliding is represented by  $F_u$  and  $F_r$ , respectively. The heat flux densities in the corresponding contact areas of the balls and outer raceway are represented by  $w_1$  and  $w_2$ , the heat flux densities in the corresponding contact areas of the balls and inner raceway are represented by  $w_3$  and  $w_4$ , the heat flux density in the non-contact area of the balls is represented by  $w_5$ , and the contact surface areas of the balls with the inner and outer raceways are represented by  $X_i$  and  $X_o$ , respectively. The non-contact surface area of the balls is represented by  $X$ . The heat flux density between the various parts of the bearing can be calculated based on the following formula:

$$w_1 = w_2 = \frac{0.25F_k}{X_o} \quad (20)$$

$$w_3 = w_4 = \frac{0.25F_k}{X_i} \quad (21)$$

$$w_5 = \frac{F_u + F_r}{X} \quad (22)$$

In summary, the following boundary conditions can be set for the steady-state temperature field analysis of the bearing:

Condition 1:  $w_1$ ,  $w_2$ ,  $w_3$ ,  $w_4$ , and  $w_5$  are directly applied to the solid elements of the high-speed bearing finite element model.

Condition 2: Convective loads are applied to the contact areas of the high-speed bearing's inner and outer raceways and the surface effect elements of the balls. The aforementioned areas are also subjected to thermal convection, while

convective loads are directly applied to the solid elements in other surface areas of the bearing.

#### 4. EXPERIMENTAL RESULTS AND ANALYSIS

This article first analyzes the temperatures of various parts of high-speed bearings under different actual working conditions, setting the axial load of the bearing at 0N, 150N, and 300N, the radial load at 200N, and the rotation speed variation range at [3000r/min, 10000r/min]. Since the friction torque of high-speed bearings is less affected by radial load, the change in temperature rise is not significant. Figures 4-6 show the temperature variation curves of the high-speed bearing balls, inner raceway, and outer raceway at different rotation speeds.

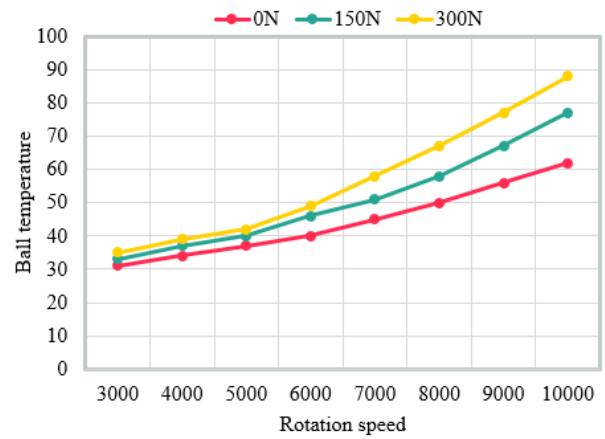


Figure 4. Temperature variation curve of high-speed bearing balls at different rotation speeds

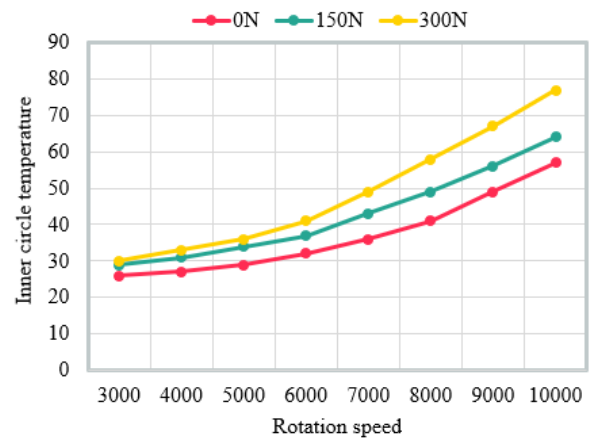
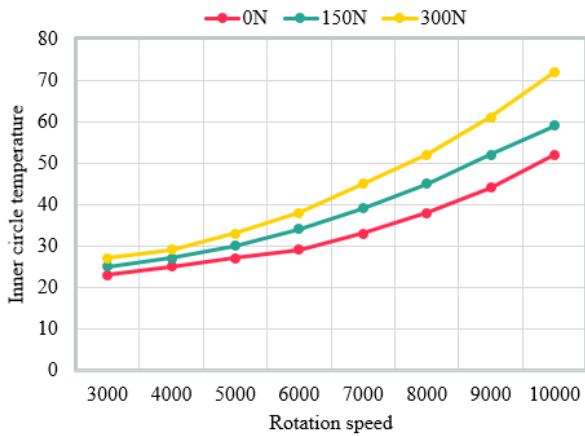


Figure 5. Temperature variation curve of high-speed bearing inner raceway at different rotation speeds

As can be seen from Figures 4-6, the temperatures of the inner and outer rings and rolling elements of the bearing continue to increase with the increase in the rotational speed of the inner ring of the high-speed bearing. The faster the speed increases, the more significant the temperature rise of the bearing. The main reason is that during high-speed operation, the frictional force between the inner and outer rings and rolling elements of the bearing increases, resulting in an increase in frictional heat generation. As the speed increases, the rate of frictional heat generation also increases, causing the bearing temperature to rise. With the increase in speed, the

flow rate of the lubricating oil inside the bearing accelerates, which may lead to a reduction in the thickness of the lubricating oil film, making the contact between the internal components of the bearing more intimate, and thereby generating more frictional heat. In addition, lubricating oil is more likely to oxidize and decompose at high speeds, reducing its lubrication performance. At the same time, during high-speed operation, the heat conduction effect between the inner and outer rings and rolling elements of the bearing is enhanced, allowing heat to be transferred more quickly to various parts of the bearing. Therefore, to reduce the temperature rise of the bearing, measures such as improving bearing design, choosing suitable lubricants, and optimizing the working environment can be taken to reduce frictional heat generation and improve heat dissipation.



**Figure 6.** Temperature variation curve of high-speed bearing outer raceway at different rotation speeds

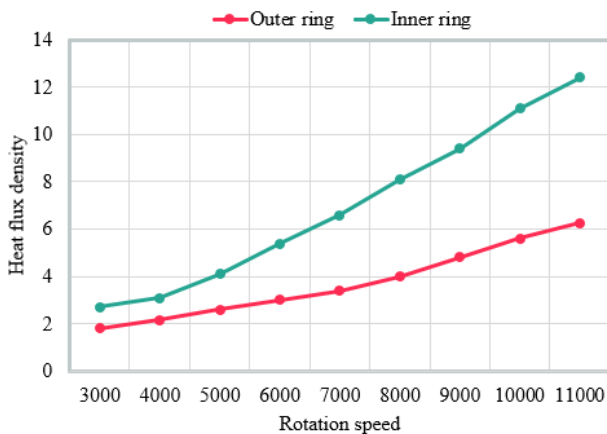


**Figure 7.** Temperature variation curve of high-speed bearing inner and outer raceways at different rotation speeds

Figure 7 shows the change curves of the heat flux density of the inner and outer rings of the high-speed bearing raceway at different speeds, and Figure 8 displays the change in the heat generation of the high-speed bearing balls at different speeds. First, we can observe that at different speeds, the heat flux density change curves of the inner and outer rings of the high-speed bearing raceway exhibit certain patterns. With the increase in speed, the heat flux density of the inner and outer rings gradually increases, which is mainly due to the increase in frictional heat generation at high speeds and the reduction in the thickness of the lubricating oil film, among other factors. In some specific speed ranges, heat flux density may fluctuate,

which may be related to bearing material properties, lubrication conditions, and other factors.

Secondly, at different speeds, the heat generation of high-speed bearing balls also shows a noticeable change trend. With the increase in speed, the heat generation of the balls usually exhibits a linear or near-linear growth trend. This is because at high speeds, the frictional force between the balls and the raceway increases, leading to an increase in frictional heat generation. In addition, at high speeds, the aerodynamic loss of the balls also increases, further contributing to the increase in heat generation. By analyzing the change curves of the heat flux density of the inner and outer rings of the high-speed bearing raceway at different speeds and the change in heat generation of the balls, we can further generate dynamic boundary conditions based on different heat generation power at different speeds. These dynamic boundary conditions can be applied to finite element analysis software for more accurately simulating the thermal characteristics of high-speed bearings at different speeds. In practical applications, these dynamic boundary conditions can guide bearing designers in considering the thermal performance of bearings at different speeds when designing bearings, thereby optimizing bearing design and usage.

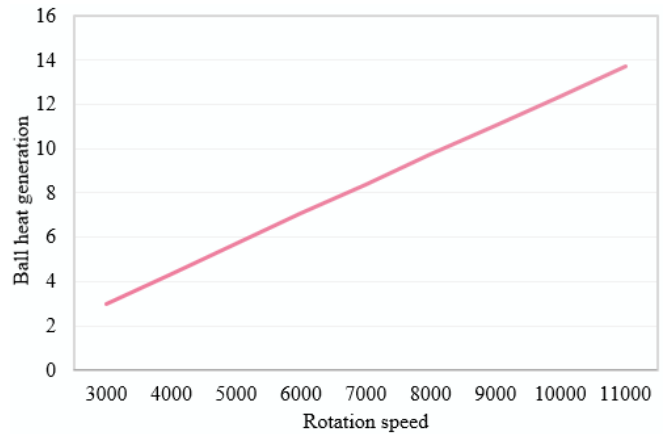


**Figure 8.** Heat generation of high-speed bearing balls at different rotation speeds

Next, this paper conducts a transient temperature field analysis of the high-speed bearing under the same external temperature conditions as the experiment. Figure 9 shows the comparison between the theoretical calculation results and the experimental calculation results of the temperature change curve of the inner ring of the high-speed bearing raceway in the transient temperature field analysis. It can be seen that in the high-speed bearing transient temperature field analysis, comparing the theoretical calculation results with the experimental calculation results of the inner ring temperature change curve helps to verify the accuracy and reliability of the high-speed bearing temperature field analysis model constructed in this paper. Through comparative analysis, we find that the theoretical calculation results and the experimental calculation results have a high consistency throughout the entire operation process.

First, during the bearing start-up phase, the inner ring temperature gradually increases, and both the theoretical calculation results and the experimental calculation results show a similar growth trend. This indicates that the model constructed in this paper can better describe the change rules of the inner ring temperature during the bearing start-up

process. Secondly, when the bearing reaches a stable operating stage, the inner ring temperature tends to stabilize, and the difference between the theoretical calculation results and the experimental calculation results is relatively small. This further confirms the accuracy of the high-speed bearing temperature field analysis model constructed in this paper under steady-state conditions. Finally, when the bearing load or speed changes, both the theoretical calculation results and the experimental calculation results can respond to these changes and show similar change trends. This indicates that the model constructed in this paper has good adaptability when dealing with dynamic operating conditions.

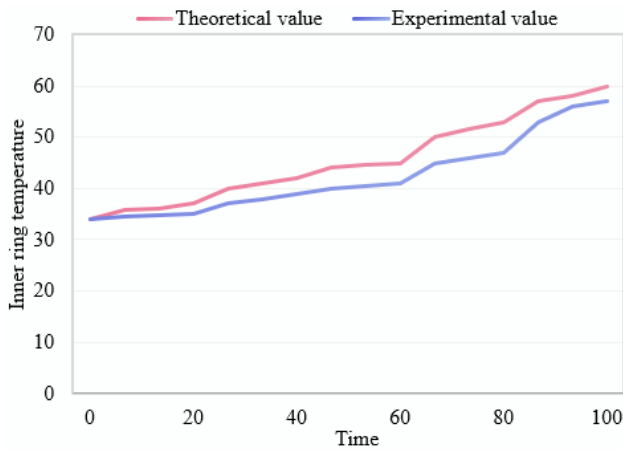


**Figure 9.** Transient temperature field analysis of high-speed bearings: inner raceway temperature variation curve

**Table 1.** Comparison of equivalent stress in bearings under different axial loads

Load	Equivalent stress		Percentage increase
	Contact analysis	Coupled field analysis	
1000N	405.6 Mpa	442.4 Mpa	9.3%
2000N	587.2 Mpa	648.5 Mpa	13%
3000N	752.6 Mpa	913.5 Mpa	20.6%
4000N	813.5 Mpa	1072.3 Mpa	31.5%

**Table 2.** Comparison of equivalent strain in bearings under different axial loads

Load	Mises equivalent strain		Percentage increase
	Contact analysis	Coupled field analysis	
1000N	0.002543	0.002145	10.6%
2000N	0.003545	0.005145	14.1%
3000N	0.003846	0.004154	16.4%
4000N	0.004354	0.005123	22.0%

Finally, this article carries out a thermal-stress coupled analysis of high-speed bearings. Tables 1 and 2 show the comparison of equivalent stress and equivalent strain in bearings under different axial loads, with the axial load in the experiment varying from 1000N to 4000N. It can be clearly seen that compared to a single contact analysis, the thermal-stress coupled field analysis obtains larger bearing stress and strain. As the axial load increases, the stress and strain of the high-speed bearing also increase. The main reason is that the internal temperature of the bearing and the temperature difference between components increase with the increase of

axial load, making the thermal stress and thermal deformation caused by the bearing temperature field more severe.

## 5. CONCLUSION

This article conducts a temperature field analysis of high-speed bearings considering the interaction of frictional heat generation. First, the motion rules of the bearing and the mechanism of friction generation are analyzed, and a high-speed bearing friction heat generation calculation analysis model suitable for actual working conditions is constructed. Then, based on ANSYS finite element analysis software, a temperature field analysis is carried out on high-speed bearings, and the internal temperature field distribution rules are obtained by exploring the effects of self-spinning, rotation speed, and external load on the temperature field. The article, combined with experiments, presents the temperature variation curves of high-speed bearing balls, inner raceways, and outer raceways at different rotation speeds. It can be seen from the comparison that the greater the axial load of the bearing, the greater the frictional heat generation of the inner and outer rings and balls, and the more apparent the temperature rise. The temperature variation curves of the inner and outer raceways of high-speed bearings at different rotation speeds are drawn, and the changes in the heat generation of high-speed bearing balls at different rotation speeds are analyzed, which can further generate dynamic boundary conditions based on different heat generation power under different rotation speeds. A comparison of theoretical and experimental calculation results for the transient temperature field analysis of high-speed bearing inner raceway temperature variation curves is carried out. This validates that the high-speed bearing temperature field analysis model constructed in this article can well reflect the change in the inner ring temperature of the bearing, and the analysis results can provide a reference for the processing and application of high-speed bearings under actual working conditions. Finally, this article carries out a thermal-stress coupled analysis of high-speed bearings and presents the analysis conclusions.

## REFERENCES

- [1] Tatar, A., Baker, A.M., Dowden, D.M. (2023). A generalized method for numerical modeling of seismically resilient friction dampers using flat slider bearing element. *Engineering Structures*, 275: 115248. <https://doi.org/10.1016/j.engstruct.2022.115248>
- [2] Oh, Y.P., Ismail, M.A.M. (2023). Pile length optimization by using shaft friction and end bearing curves developed from instrumented pile load test. *Physics and Chemistry of the Earth, Parts A/B/C*, 129: 103278. <https://doi.org/10.1016/j.pce.2022.103278>
- [3] Huang, L., Zeng, B., Zhou, Z., Zhang, W., Wei, Y., Li, C. (2023). Seismic behavior and reliability of variable friction damped self-centering prestressed concrete frames considering bolt bearing. *Soil Dynamics and Earthquake Engineering*, 164: 107643. <https://doi.org/10.1016/j.soildyn.2022.107643>
- [4] Wang, H., Wang, X., Liu, Z. (2022). Experimental study on friction characteristics of surface textured rubber slats on water-lubricated bearing. In *International Conference*

- on Mechanical Design and Simulation (MDS 2022), 12261: 1203-1212. <https://doi.org/10.1117/12.2640998>
- [5] Liu, Z., Fu, Y., Zheng, S. (2022). Development and experimental analysis of friction torque testing machine for planetary thread roller bearing. *Journal of Physics: Conference Series*, 2383: 012123. <https://doi.org/10.1088/1742-6596/2383/1/012123>
- [6] Dai, L. (2022). Experimental study on friction torque calibration of mechanical seal main bearing. *International Conference on Mechanisms and Robotics*, 12331: 567-572. <https://doi.org/10.1117/12.2652452>
- [7] Wang, K., Wu, C., Zhang, H., Li, J., Li, J. (2022). Cylindrical bearing inspired oil enhanced rolling friction based nanogenerator. *Nano Energy*, 99: 107372. <https://doi.org/10.1016/j.nanoen.2022.107372>
- [8] Cao, Y., Liu, C., Zhu, S., Yu, J. (2019). Temperature Field Analysis and Optimization of the Homopolar Magnetic Bearing. *Progress Electromagnetics Research M*, 85: 105-114. <http://dx.doi.org/10.2528/PIERM19072801>
- [9] Zhou, X., Zhu, Q., Wen, B., Zhao, G., Han, Q. (2019). Experimental investigation on temperature field of a double-row tapered roller bearing. *Tribology Transactions*, 62(6): 1086-1098. <https://doi.org/10.1080/10402004.2019.1649509>
- [10] Zhang, Y.Q., Sun, J.C., Kong, P.R., Kong, X.B., Yu, X.D. (2019). Research on the oil film temperature field of hydrostatic bearing with variable viscosity dynamic simulation and experiment. *Proceedings of the Institution of Mechanical Engineers, Part J: Journal of Engineering Tribology*, 233(11): 1763-1772. <https://doi.org/10.1177/1350650119846002>
- [11] Shi, J.X., Luo, J., Jiang, Z.Y. (2018). Temperature field monitoring of mass concrete of i-shaped bearing platform. *IOP Conference Series: Materials Science and Engineering*, 423: 012123. <https://doi.org/10.1088/1757-899X/423/1/012123>
- [12] Cristea, A.F., Bouyer, J., Fillon, M., Pascovici, M.D. (2017). Transient pressure and temperature field measurements in a lightly loaded circumferential groove journal bearing from startup to steady-state thermal stabilization. *Tribology Transactions*, 60(6): 988-1010. <https://doi.org/10.1080/10402004.2016.1241330>
- [13] Kou, S.Q., Gao, Y., Zhao, Y. (2017). Numerical simulation and experimental validation of the temperature field generated during pulsed laser processing of notches for fracture splitting of an engine crankcase main bearing seat. *Lasers in Engineering (Old City Publishing)*, 37(1-3): 177-195.
- [14] Guo, C., Cui, Y. (2016). Study on the hydrostatic slide film temperature field and bearing capacity of precision grinding machine. In *Proceedings of the 5th International Conference on Electrical Engineering and Automatic Control*, pp. 717-724. [https://doi.org/10.1007/978-3-662-48768-6\\_80](https://doi.org/10.1007/978-3-662-48768-6_80)
- [15] Kovács, K., Kamnev, A.A., Pechoušek, J., Tugarova, A. V., Kuzmann, E., Machala, L., Zbořil, R., Homonnay, Z., Lázár, K. (2016). Evidence for ferritin as dominant iron-bearing species in the rhizobacterium *Azospirillum brasilense* Sp7 provided by low-temperature/in-field Mössbauer spectroscopy. *Analytical and bioanalytical chemistry*, 408: 1565-1571. <https://doi.org/10.1007/s00216-015-9264-3>
- [16] Chen, J., Ma, J., Fang, Y., Li, T., Li, J. (2015). Analysis of temperature field distribution of magnetic-fluid bearing for high-speed trains. In *2015 18th International Conference on Electrical Machines and Systems (ICEMS)*, Pattaya, Thailand, pp. 620-623. <https://doi.org/10.1109/ICEMS.2015.7385110>
- [17] Zhou, X., Shen, Y., Wang, M. (2020). Temperature Field Analysis and Optimization of Radial 2-DOF Hybrid Magnetic Bearing. *Progress In Electromagnetics Research M*, 98: 45-54. <http://dx.doi.org/10.2528/PIERM20081101>
- [18] Hasnain, J., Abbas, Z., Sheikh, M., Aly, S. (2020). Analysis of dusty Casson fluid flow past a permeable stretching sheet bearing power law temperature and magnetic field. *International Journal of Numerical Methods for Heat & Fluid Flow*, 30(6): 3463-3480. <https://doi.org/10.1108/HFF-11-2018-0685>
- [19] Zou, Y., Bian, X., Shang, J., Guan, X., Wu, J., Li, Q. (2020). Calculation and measurement of the magnetic field of Nd<sub>2</sub>Fe<sub>14</sub>B magnets for high-temperature superconducting magnetic bearing rotor. *Journal of Superconductivity and Novel Magnetism*, 33: 931-940. <https://doi.org/10.1007/s10948-019-05310-6>
- [20] Liska, T., Swetz, A., Lai, P.N., Zeller, M., Teets, T.S., Gray, T.G. (2020). Room-temperature phosphorescent platinum (II) alkynyls with microsecond lifetimes bearing a strong-field pincer ligand. *Chemistry-A European Journal*, 26(38): 8417-8425. <https://doi.org/10.1002/chem.202000500>
- [21] Chen, S., Rong, X., Bao, X., Li, S., Li, C., Chen, Z., Wei, L. (2023). Research on temperature field during the hot pressing process of UHMWPE-based water-lubricated bearing. *International Journal of Polymer Analysis and Characterization*, 28(1): 1-11. <https://doi.org/10.1080/1023666X.2022.2138131>
- [22] Wang, L., Pan, Y., Jiang, Z., Zhang, Y., Fu, X., Men, X. (2022). Temperature field analysis of cylindrical roller bearing based on rheological properties of grease. In *Proceedings of the 14th International Conference on Computer Modeling and Simulation, Chongqing, China*, pp. 115-120. <https://doi.org/10.1145/3547578.3547596>
- [23] Chen, J., Zhang, W., Wang, H. (2021). Intelligent bearing structure and temperature field analysis based on finite element simulation for sustainable and green manufacturing. *Journal of Intelligent Manufacturing*, 32: 745-756. <https://doi.org/10.1007/s10845-020-01702-x>
- [24] Bao, H., Hou, X., Tang, X., Lu, F. (2021). Analysis of temperature field and convection heat transfer of oil-air two-phase flow for ball bearing with under-race lubrication. *Industrial Lubrication and Tribology*, 73(5): 817-821. <https://doi.org/10.1108/ILT-03-2021-0067>